Proc. 7th Int. Symp. on Engineering Turbulence Modelling and Measurements - ETMM7
Limassol, Cyprus, 4-6 June 2008

MANIPULATION OF THE LARGE-SCALE STRUCTURE IN WALL TURBULENCE FOR TURBULENT WALL-FRICTION-DRAG REDUCTION

Koji Fukagata[1], Michio Kobayashi[2] and Nobuhide Kasagi[2]

[1]Department of Mechanical Engineering, Keio University
[2] Department of Mechanical Engineering, The University of Tokyo

fukagata@mech.keio.ac.jp

Abstract

Direct numerical simulation (DNS) of a turbulent channel flow is performed in order to explore the possibility of wall-friction-drag reduction through the manipulation of large-scale structure. As an idealized feedback control, we selectively damp either the small-scale wall-normal velocity fluctuations (defined as those with spanwise wavelength smaller than 300 wall units) or the large-scale fluctuations (spanwise wavelength larger than 300 wall units). The present DNS shows that the control of small-scale fluctuations is more efficient than that of large-scale fluctuations. When the small-scale fluctuation is damped, the friction drag reduces simply according to the absence of small-scale fluctuations. When the large-scale fluctuations are damped, in contrast, the small-scale fluctuations are drastically increases and the reduction of friction drag is less than that expected from the absence of large-scale fluctuations. This increase of small-scale fluctuations is found to be due to the reduction of pressure fluctuations and weakened destruction of Reynolds shear stress.

1 Introduction

Since 1990's, extensive research has been made on the feedback control of wall-bounded turbulent flows for skin friction drag reduction (see, e.g., Kasagi, 1998; Bewley 2001; Kim, 2003; and Kim and Bewley, 1997). While different schemes, such as those based on the physical argument (e.g., Choi et al., 1994), and the modern control theory (e.g., Bewley et al., 2001), have been examined, a common mechanism for successful drag reduction is attenuation of the quasi-streamwise vortices in the region near the wall. This should be reasonable because the Reynolds number considered in these studies is relatively low (typically $Re_\tau \sim 100$, where Re_τ is the friction Reynolds number) and the Reynolds shear stress (RSS) produced by the quasi-streamwise vortices has the largest contribution to the skin friction drag.

The skin friction drag and the RSS are mathematically related by the identity equation (Fukagata et al., 2002). For a fully developed channel flow, for instance, the identity equation reads

$$C_f = \frac{12}{\mathrm{Re}_b} + 24\int_0^1 (1-y)(-\overline{u'v'})dy. \qquad (1)$$

Here, all the quantities are made dimensionless by using the channel half-width and twice the bulk mean velocity, and Re_b is the bulk Reynolds number. The first term is the laminar friction drag, and the second term is the turbulent contribution, which is an integral of RSS $(-\overline{u'v'})$ weighted by the distance from the channel centerline $(1-y)$.

Equation (1) suggests that, at large Reynolds numbers, the contribution of RSS in the region far from the wall (i.e., in the central region of channel) becomes dominant, unlike the case of low Reynolds number flows so far studied. Figure 1 shows the profiles of weighted RSS, $(1-y)(-\overline{u'v'})$ (i.e., integrand of the second term in Eq. (1)) in uncontrolled flow at different Reynolds numbers. At higher Reynolds numbers, the contribution of near-wall RSS to the friction drag drastically decreases and the contribution of the RSS far from the wall becomes dominant.

The RSS in the region far from the wall is closely related to the so-called large-scale structure. According to the recent PIV (Tomkins and Adrian, 2005) and direct numerical simulation (DNS) (Abe et al., 2004; Iwamoto et al., 2004) of moderately high Reynolds number wall-bounded flows, this large-scale structure has a spatial scale of about channel half-width. Although the attenuation of small-scale structure in the region near the wall may lead to significant drag reduction even at practically high Reynolds numbers, as theoretically predicted by Iwamoto et al. (2005), the large-scale structure can be considered as an alternative target of control for friction drag reduction at high Reynolds numbers. Friction drag reduction by the manipulation of the large-scale structure, if possible, is also beneficial in terms of hardware development, because the requirement for the size of sensors and actuators (which is as small as 30 wall units for the conventional feedback control and it corresponds to the order of 100 μm in the typical applications, such as high-speed train) can be largely relaxed. Therefore, in the present study, we investigate by means of numerical experiments the possibility of friction drag

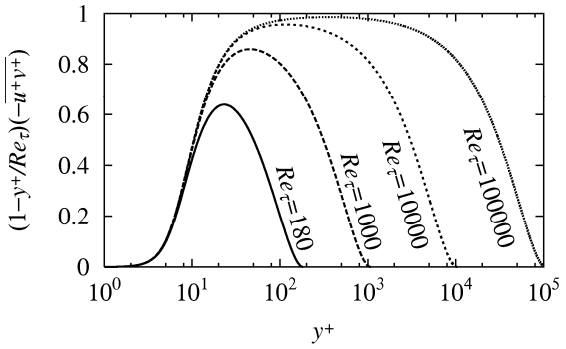

Figure 1: Distribution of weighted Reynolds shear stress at different Reynolds number (calculation using the eddy viscosity model with the van Driest damping function.)

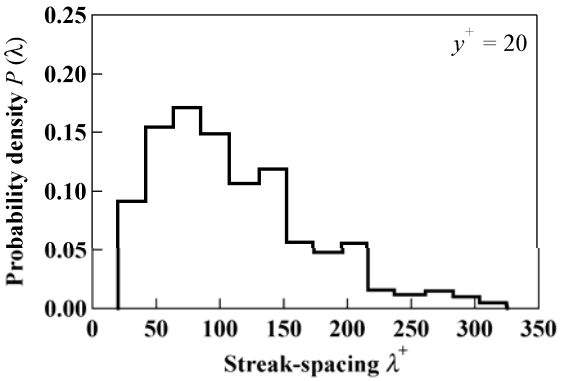

Figure 2: Probability density histograms of spanwise streak spacing for Re_θ = 2030 (Smith & Metzler, 1983).

reduction by the manipulation of large-scale structure.

2 Direct numerical simulation

We consider a fully developed turbulent channel flow. The flow rate is kept constant. The Reynolds number based on the bulk-mean velocity and the channel width is $\mathrm{Re}_b = 2U_b\delta/\nu = 24000$ and the corresponding friction Reynolds number in the uncontrolled case is $\mathrm{Re}_\tau \approx 640$.

The present DNS is performed by using a pseudo-spectral code (Iwamoto et al., 2004). It is based on the wall-normal velocity and vorticity formulation similar to that by Kim et al. (1987). Fourier expansion is used for the streamwise (x) and spanwise (z) directions with the periodic boundary condition. Chebychev-tau method is used for the wall-normal (y) direction. The no-slip condition is imposed on the wall. The fourth order accurate Runge-Kutta method is used for the temporal integration.

The computational domain is $2.5\pi \times 2\delta \times \pi\delta$ and the number of nodes are 288 × 257 × 384 in x, y, and z directions, respectively. The corresponding grid size is $\Delta x^+ = 17.7$, $\Delta z^+ = 5.3$ in the streamwise and spanwise directions, respectively. The minimum grid size in the wall-normal direction is $\Delta y_{\min}{}^+ = 0.049$. Hereafter, the superscript of "+" denotes the wall unit in the uncontrolled flow.

3 Control method

As an ideal control input for suppression of velocity fluctuations, we consider a feedback body force which works as a damper. This damper is added to the wall-normal component of the momentum equation, and the wall-normal momentum equations is modified to read

$$\frac{\partial v}{\partial t} = -\vec{u}\cdot\nabla v - \nabla p + \frac{1}{\mathrm{Re}_b}\nabla^2 v - \frac{\alpha}{\tau}v, \qquad (2)$$

where τ is the relaxation time (set here at 10 wall unit time). The prefactor α takes a value of 0 or 1 depending on the spanwise wavenumber λ_z. We set either:

- $\alpha = 0$ (for $\lambda_z \le \lambda_c$) and $\alpha = 1$ (for $\lambda_z > \lambda_c$) to damp the large-scale structure only, or
- $\alpha = 0$ (for $\lambda_z > \lambda_c$) and $\alpha = 1$ (for $\lambda_z \le \lambda_c$) to damp the small-scale structure only.

The threshold wavenumber λ_c is chosen so as to separate the small and large scale structures. As shown in Fig. 2, the spanwise size of the near-wall streaky structure is known to be less than 300 wall unit length. Therefore, λ_c is set here at 300 wall unit. In the uncontrolled flow under the present condition, the amounts of turbulent kinetic energy (TKE) contained below and above λ_c are found to be about 2/3 (large-scale) and 1/3 (small-scale) of the total TKE, respectively.

For notational simplicity, the two examined cases are hereafter referred to as:

- Case SMALL, the case where the small-scale structure is damped;
- Case LARGE, the case where the large-scale structure is damped.

4 Results and discussions

Figure 3 shows the time trace of the drag reduction rate, R_D, defined as

$$R_D = 1 - \frac{\left(-\overline{dp/dx}\right)_{\text{control}}}{\left(-\overline{dp/dx}\right)_{\text{no control}}}. \qquad (3)$$

While Case SMALL reaches a quasi-steady state after $t^+ \sim 100$, a longer time ($t^+ \sim 1000$) is required for the drag in Case LARGE to be converged. The drag reduction rates in the quasi-steady states are R_D = 27% in Case LARGE and R_D = 43% in Case SMALL.

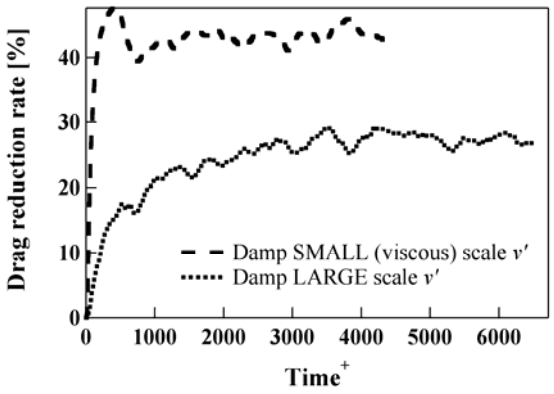

Figure 3: Time trace of drag reduction rate.

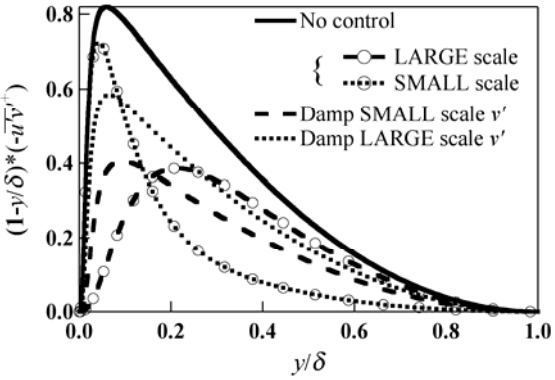

Figure 4: Distribution of weighted Reynolds shear stress.

Figure 4 shows the weighted RSS profiles. As indicated in Eq. (1), the area enclosed by each curve and the horizontal axis is directly proportional to the turbulent contribution of friction drag. Although the weighted RSS is reduced in both cases, more reduction is found in Case SMALL. Remembering the present condition that the only one third of TKE was originally contained in small-scale, damping of the small-scale fluctuation can be considered more efficient for the friction drag reduction. The figure also shows two more lines with circles. These are the large-scale and small scale-components in the no-control case. Although the weighted RSS profile in Case SMALL is not the same as that of large-scale component of the no-control case, the area (i.e., turbulent contribution to the friction drag) looks nearly unchanged. In contrast, the weighted RSS in Case LARGE has larger value far from the wall than that of small-scale component of the no-control case, and the area increases accordingly.

The difference in these drag reduction effects is better explained by Figure 5(a), which shows the integrated contributions of RSS to the skin friction drag (i.e., the second term of Eq. (1)) decomposed into the small and large spanwise wavenumber components. Without control, 91% of the total friction drag is the turbulent contribution; 55% of that is the large-scale components, and 45% of that is the small-scale components. When the small-scale fluctuations are damped, the contribution from the

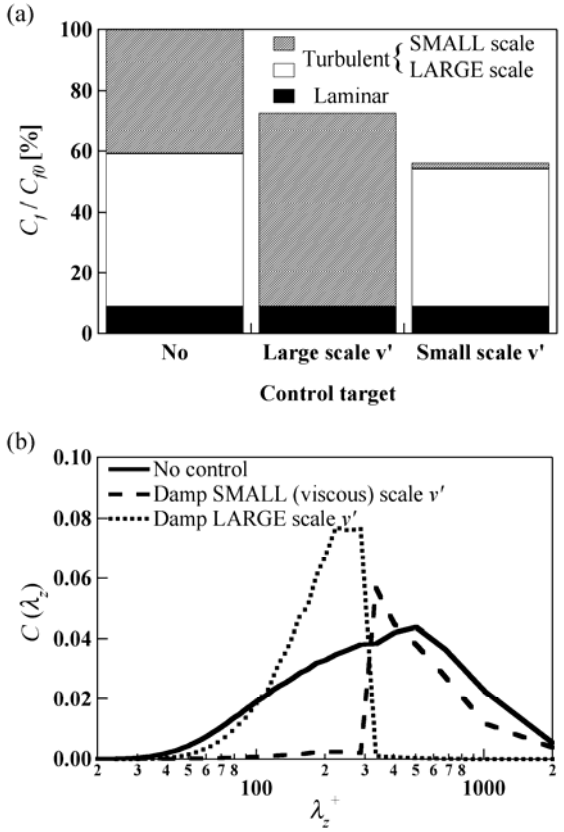

Figure 5: (a) Contribution to friction drag; (b) Premultiplied co-spectra of turbulent friction term.

large-scale component (light gray) is nearly unchanged. In contrast, when the large-scale fluctuations are damped, the contribution from the small-scale component (dark gray) is almost doubled.

More detailed explanation can be given by further decomposing the turbulent contribution into each wavenumber λ_z. Namely, we introduce the following premultiplied and weighted co-spectrum:

$$C(\lambda_z) \equiv (\frac{\delta}{\lambda_z})\int_0^1 (1-\frac{y}{\delta})(-\overline{\hat{u}' * \hat{v}'})d(\frac{y}{\delta}), \qquad (4)$$

where the hat indicates the Fourier transform in the spanwise direction. Figure 5(b) shows this co-spectrum. In Case SMALL, the damped component ($\lambda_z{}^+ < 300$) is simply cut out, while the undamped component ($\lambda_z{}^+ > 300$) remains nearly unchanged. In Case LARGE, in contrast, there is a pile-up in $\lambda_z{}^+ < 300$. This pile-up is related to the increase of the weighted RSS in the region far from the wall, as has been observed in Fig. 4.

Figure 6 shows the root-mean-square (rms) values of the velocity fluctuations. In the region near the wall, the streamwise and spanwise rms velocity components are nearly unchanged (or slightly increased) in Case SMALL, while it is slightly decreased in Case LARGE, as compared to the uncontrolled case. In the region far from the wall, all the

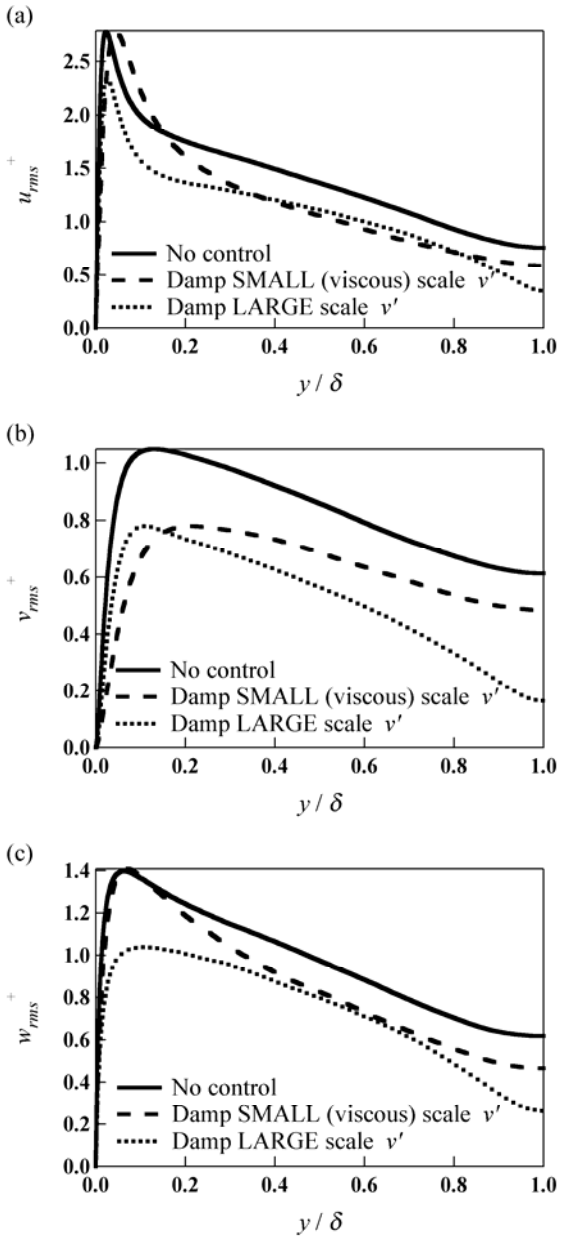

Figure 6: Rms velocity fluctuations. (a) u_{rms}; (b) v_{rms}; (c) w_{rms}.

rms velocity components are decreased in both cases. They decrease more in Case LARGE than in Case SMALL. This looks inconsistent with the trend in the RSS, where larger reduction is observed in Case SMALL. The reason for this discrepancy can be explained by the correlation coefficient between *u* and *v*. As shown in Fig. 7, the correlation is significantly raised in Case LARGE, and this stronger correlation results in the larger RSS despite the smaller rms velocities.

According to the recent analysis by Frohnapfel et al. (2007), the drag reduction by additives (such as polymers and fibers) is related to the increase of anisotropy towards the one-component limit in the near-wall region. The second and third invariants of the anisotropy tensor a_{ij},

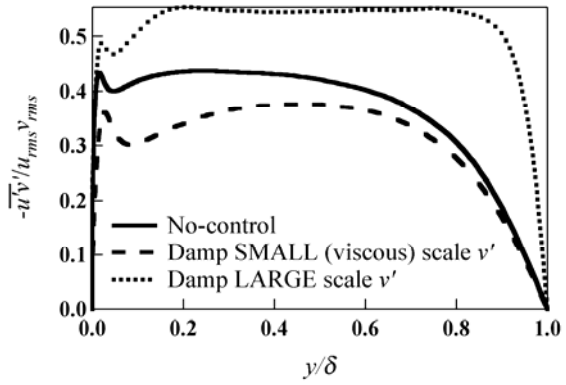

Figure 7: Correlation coefficient of $-\overline{u'v'}$.

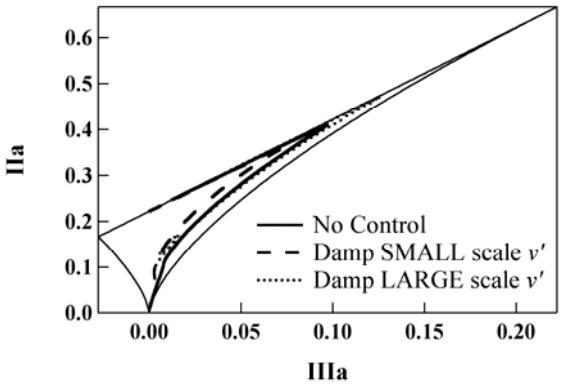

Figure 8: Anisotropy invariant map.

$$a_{ij} = \frac{\overline{u_i u_j}}{u_k u_k} - \frac{1}{3}\delta_{ij}, \tag{5}$$

are defined as

$$II_a = a_{ij}a_{ji}, \tag{6}$$

$$III_a = a_{ij}a_{jk}a_{ji}, \tag{7}$$

respectively. Figure 8 shows the anisotropy invariant map in the present three cases. The anisotropy in the near-wall region in Case LARGE shifts toward the

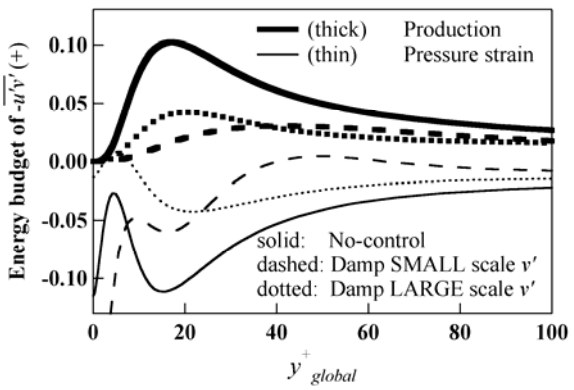

Figure 9: Production and Pressure strain terms of $-\overline{u'v'}$ budget.

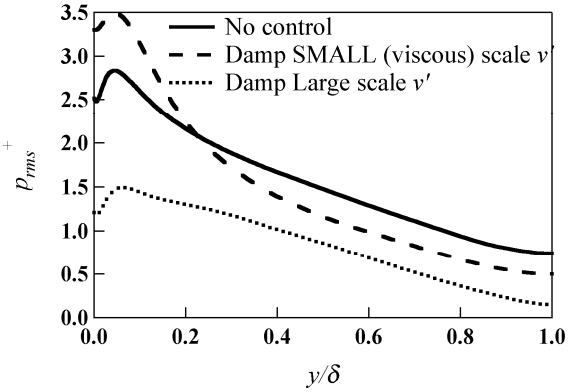

Figure 10: Rms pressure fluctuations.

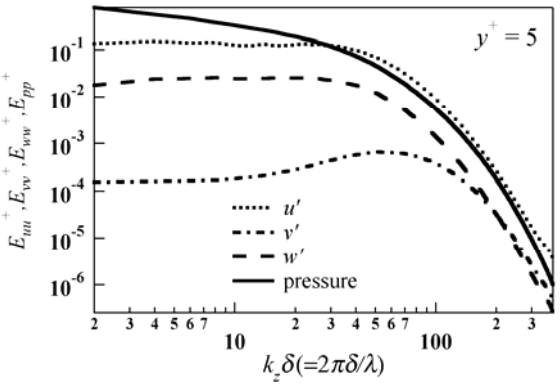

Figure 11: Spanwise power spectra of velocity and pressure in the uncontrolled case.

one-component limit (right top), which is similar to to the drag reduction by additives. In contrast, that in Case SMALL moves away from the one-component limit, despite that the drag reduction rate is higher than Case LARGE. It indicates that the general trend that holds for drag reduction by additives does not hold for the present cases.

In order to investigate the mechanism in the change of RSS, we examine the budget of RSS expressed as follows:

$$\frac{D}{Dt}\left(\overline{-u_1'u_2'}\right) = \underbrace{\overline{u_2'^2}\frac{\partial \overline{u_1}}{\partial x_2}}_{\langle \mathrm{P}\rangle} \underbrace{-\frac{1}{\rho}\left(\overline{p'\frac{\partial u_1'}{\partial x_2}} + \overline{p'\frac{\partial u_2'}{\partial x_1}}\right)}_{\langle \mathrm{PS}\rangle} + \underbrace{\frac{1}{\rho}\left\{\frac{\partial}{\partial x_2}\left(\overline{u_1' p'}\right) + \frac{\partial}{\partial x_1}\left(\overline{u_2' p'}\right)\right\}}_{\langle \mathrm{PD}\rangle} \underbrace{-\nu\frac{\partial^2}{\partial x_k \partial x_k}\left(\overline{u_1' u_2'}\right) + \frac{\partial}{\partial x_k}\left(\overline{u_1' u_2' u_k'}\right)}_{\langle \mathrm{VD}\rangle \qquad \langle \mathrm{TD}\rangle} \underbrace{-2\nu\overline{\frac{\partial u_1'}{\partial x_k}\frac{\partial u_2'}{\partial x_k}}}_{\langle \mathrm{D}\rangle} \tag{8}$$

Figure 9 shows the profiles of the production <P> and the pressure strain <PS> terms in Eq. (8). These terms are significantly reduced in both cases according to the drag reduction. The noteworthy observation in the near-wall region is that the production is stronger and the pressure-strain is weaker in Case LARGE than those in Case SMALL. The larger production is simply related to the larger wall-normal velocity fluctuations as observed in Fig. 6(b). The weaker pressure-strain in Case LARGE is conjectured to be due to the smaller pressure fluctuations as shown below.

Figure 10 shows the rms pressure fluctuations. While the rms pressure fluctuation in the region near the wall is increased in Case SMALL, that in Case LARGE is significantly reduced. This reduction is related to the fact that the pressure field has relatively large spatial scale as shown in Fig. 11. Namely, the pressure fluctuations have been selectively weakened by the damping of the large-scale fluctuations.

Finally, the instantaneous vortical structure in the present three cases are shown in Fig. 12. Here, the vortex core is identified by using the isosurface of the second invariant of the velocity gradient tensor, *II*. As observed in Fig. 12(b), the typical vortical structure in Case LARGE is the quasi-streamwise vortices similar to those in the uncontrolled flow (Fig. 12(a)). In Case SMALL, in contrast, the quasi-streamwise vortices is hardly be observed and spanwise vortices appears instead. This structural change may be related to the change in the anisotropy invariant as observed in Fig. 8, which moved away from the one-component limit. Note that such spanwise vortices have been observed in other feedback control (e.g., Koumoutsakos, 1999) as well as in the flow over a compliant wall (Fukagata et al., 2007), although the detailed mechanisms of its generation and its relationship to the drag reduction are still not completely clear.

5 Conclusions

We performed direct numerical simulation (DNS) of a turbulent channel flow with an idealized feedback control, which selectively damp either the small-scale wall-normal velocity fluctuations. From the present DNS results, it can be concluded that for turbulent friction drag reduction, the suppression of large-scale structure does not have merit over the attenuation of small-scale structure. The damping of large-scale fluctuations leads to reduction of the pressure fluctuations and thereby reduction of pressure-strain correlation. The reduced pressure-strain correlation results in weaker destruction of the Reynolds shear stress and it finally raises the Reynolds shear stress.

Acknowledgements

The authors are grateful to Dr. Kaoru Iwamoto (Tokyo University of Agriculture and Technology) for providing the DNS code and Dr. Yuji Suzuki (The University of Tokyo) for valuable comments.

(a)

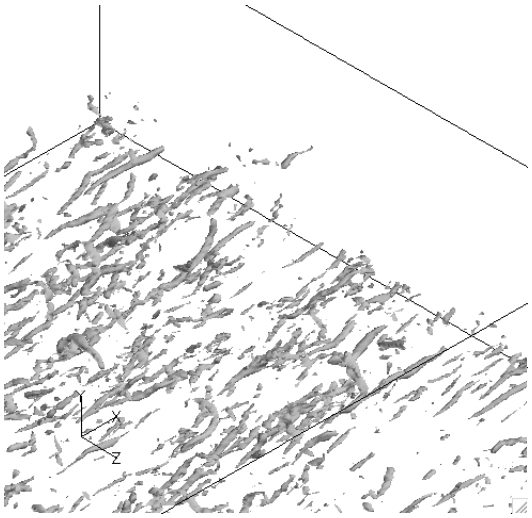

(b)

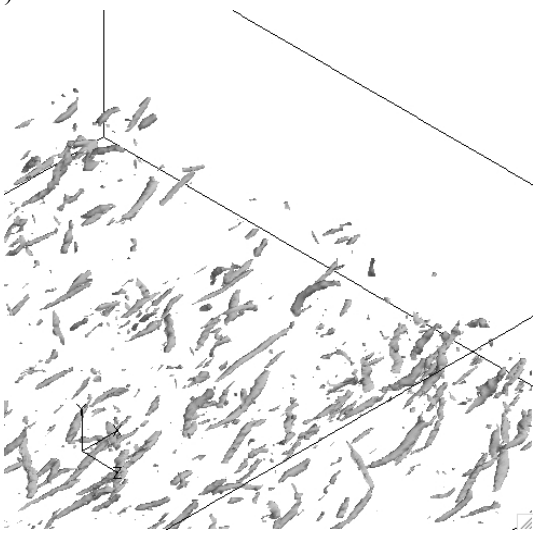

(c)

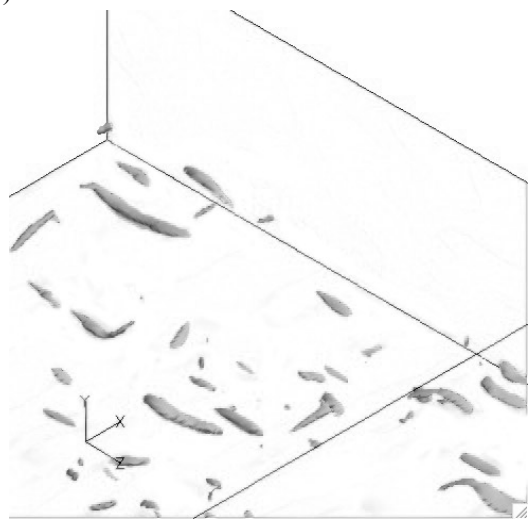

Figure 12: Instantaneous flow field. (a) No control (II^+ = -0.05); (b) Damp large scale v' (II^+ = -0.03); (c) Damp small scale v' (II^+ = -0.015). Bottom plane: wall, Upper plane: channel center.

References

Abe, H., Kawamura, H, and Choi, H. (2004), Very large-scale structures and their effects on the wall shear-stress fluctuations in a turbulent channel flow up to Re_τ = 640, *J. Fluids Eng.,* Vol. 126, pp. 835-843.

Bewley, T.R. Moin, P. and Temam, R. (2001), DNS-based predictive control of turbulence: an optimal benckmark for feedback algorithms, *J. Fluid Mech.*, Vol. 447, pp. 179-225.

Choi H., Moin P. and Kim J. (1994), Active turbulence control for drag reduction in wall-bounded flows, *J. Fluid Mech.*, Vol. 262, pp. 75-110.

Fukagata, K., Iwamoto, K., and Kasagi, N. (2002), Contribution of Reynolds stress distribution to the skin friction in wall-bounded flows, *Phys. Fluids*, Vol. 14, pp. L73-L76.

Fukagata, K., Kern, S., Chatelain, P., Koumoutsakos, P., and Kasagi, N. (2007), Optimization of an anisotropic compliant surface for turbulent friction drag reduction, Proc. 5th Int Symp. on Turbulence and Shear Flow Phenomena, Munich, Aug. 27-29, 2007, pp. 727-732.

Frohnapfel, B., Lammars, P., Jovanović, J., and Durst, F. (2007), Interpretation of the mechanism associated with turbulent drag reduction in terms of anisotropy invariants, *J. Fluid Mech.*, Vol. 577, pp. 457-466.

Iwamoto, K., Fukagata, K., Kasagi, N., Suzuki, Y. (2005), Friction drag reduction achievable by near-wall turbulence manipulation at high Reynolds number, *Phys. Fluids*, Vol. 17, Art. No. 011702.

Iwamoto, K., Kasagi, N. and Suzuki Y. (2004), Dynamical roles of large-scale structures in turbulent channel flow, Computational Mechanics, WCCM VI/APCOM'04, (Springer, 2004), MS-022-174, pp. 1-7.

Kasagi, N. (1998), Progress in direct numerical simulation of turbulent transport and its control, *Int. J. Heat Fluid Flow*, Vol. 19, pp. 125-134.

Kim, J. (2003), Control of turbulent boundary layers, *Phys. Fluids*, Vol. 15, pp. 1093-105.

Kim, J. and Bewley T.R. (2007), A linear systems approach to flow control, *Annu. Rev. Fluid Mech.*, Vol. 39, pp. 383-417.

Kim, J., Moin P., and Moser, R. (1987), Turbulence statistics in fully developed channel flow at low Reynolds number, *J. Fluid Mech.* Vol. 177, pp. 133-166.

Koumoutsakos, P. (1999), Vorticity flux control for a turbulent channel flow, *Phys. Fluids* Vol. 11, pp. 248-250.

Smith, C.R. and Metzler S.P. (1983), The characteristics of low-speed streaks in the near-wall region of a turbulent boundary-layer, *J. Fluid Mech.*, Vol. 129, pp. 27-54.

Tomkins, C.D. and Adrian, R.J. (2005), Energetic spanwise modes in the logarithmic layer of a turbulent boundary layer, *J. Fluid Mech.*, Vol. 545, pp.141-162.